Activity report of the Italian CRG beamline at the European Synchrotron Radiation Facility (ESRF)

N. 8 - January 2021

Grenoble, January 2021

Responsabile editoriale: Francesco d'Acapito
(*dacapito@iom.cnr.it*)

Editing: Roberta De Donatis
(*roberta.dedonatis@cnr.it*)

ISSN 2553-9248

LISA

Annual Report 2020

Istituto Officina dei Materiali

Abstract

This document resumes the activity of the Italian CRG beamline at ESRF (LISA project) during year 2020. The latest news from the beamline are presented as well as details on the technical activity, highlight experiments and publications.

Keywords

Italian beamline at ESRF, BM08

LISA project

X-ray Absorption Spectroscopy

Index

Year 2020 has represented a tragic moment for our society with the sanitary emergency caused by the COVID-19 pandemic. Nonetheless, 2020 has also marked a turning point in the history of ESRF and synchrotron radiation science, with the completion of the EBS ring and the beginning of its operation. On Aug 25, in perfect time with the schedule, EBS has started providing to users a beam at full current (200 mA) with record values for the emittance, about 150pm horizontal and 20 pm vertical.

LISA has followed the track by completing all the interventions needed to receive the new beam, in particular the modifications of the lead shielding made necessary by the displacement of the beam several cm outwards. In particular, it revealed necessary to modify all the beam-tube passages through the lead walls and replace the shielding around the connecting tube between the first and second experimental hutches. (See Figure 1)

Figure 1: Left: a new slim shielding for the connecting tube between EH1 and EH2. Right: the refurbished shielding after the main beam shutter in the Optic Hutch.

The intervention was still ongoing when the confinement order from the French government came on March 17 and the works could be completed only in the month of June when the access restrictions at ESRF for CRGs and external companies were levied. Since then, the LISA staff has worked intensely in order to validate the beamline for radioprotection (two radiation tests on the new shielding were carried out at 5 and 200 mA, the last one by an independent external company), to realign and optimizing all the optical elements on the new beam and define the beamline parameters with the new source. The data are presented at Page 5 where it is shown that LISA fully profits from the new smaller source. The beamline was among the 26 beamlines ready to restart the user program on Aug 25 and, after some final adjustments, the first users were ‘welcomed’ (actually their samples were, as users were not allowed to come on site at the time) by September.

The mail-in mode for experiments has represented a considerable challenge for the beamline staff as it involved the development of new automatic procedures for data collection, sample changing and treatment with the aim of increasing and optimizing the use of beamtime during the full 24 h operation. The results of this effort are collected in Page 7. In the second semester of 2020 LISA has carried out 7 experimental sessions completely in mail-in mode 6 ESRF experiments and 1 CERIC experiment for a total amount of 134 shifts. Some changes were necessary at the end of October due to the new confinement order on the French territory and the consequent changes of the ESRF schedule. During the restart in August/September LISA has hosted a doctorate student, Ludovico Macera from l’Aquila University who has worked with the staff to the definition of the optimal conditions for data collection in the lowest part of the accessible energy spectrum (4-5 keV). In 2020 19 publications related to LISA were published by international journals out of which 6 on high impact journals (IF >7), as reported at Page 17.

Year 2020 brought relevant good news also on the 'legal' side. After the positive opinion of the ESRF Scientific Advisory Committee (SAC) in May 2019 for continuing the activities of LISA, a new contract has been signed between ESRF and CNR for the operation of the beamline covering the period 1/Jan/2020 -> 31/Dec/2024. As an additional opportunity for users, an agreement has been successively signed between CNR and CERIC (Central Europe Research Infrastructure Consortium) for the insertion of LISA in their list of available instruments. This will permit to widen the user community accessing LISA and provide them a financial support for those coming to Grenoble carrying out the experiment. From now on users can then apply for beamtime either on the ESRF site:

https://smis.esrf.fr/misapps/SMISWebClient/home.do

or on the CERIC site:

https://vuo.elettra.trieste.it/pls/vuo/guest.startup

First calls have been issued on September and October 2020 respectively for ESRF and CERIC and other calls will follow in 2021.

For 2021 it is foreseen the restart of the conventional user access, in the first months of the year with just one user per experiment. This rule is likely to be softened in the course of the year as soon an improvement of the sanitary situation will be ascertained.

Looking forward to see you again at LISA.

F. d'Acapito

Beam size

Thanks to the new EBS source, a beam size less than 100 µm is now available, permitting to probe very small samples. The resulting focused beam area is about 10 times smaller respect to the previous ESRF source. Figure 2 shows a comparison of the beam size between the two sources:

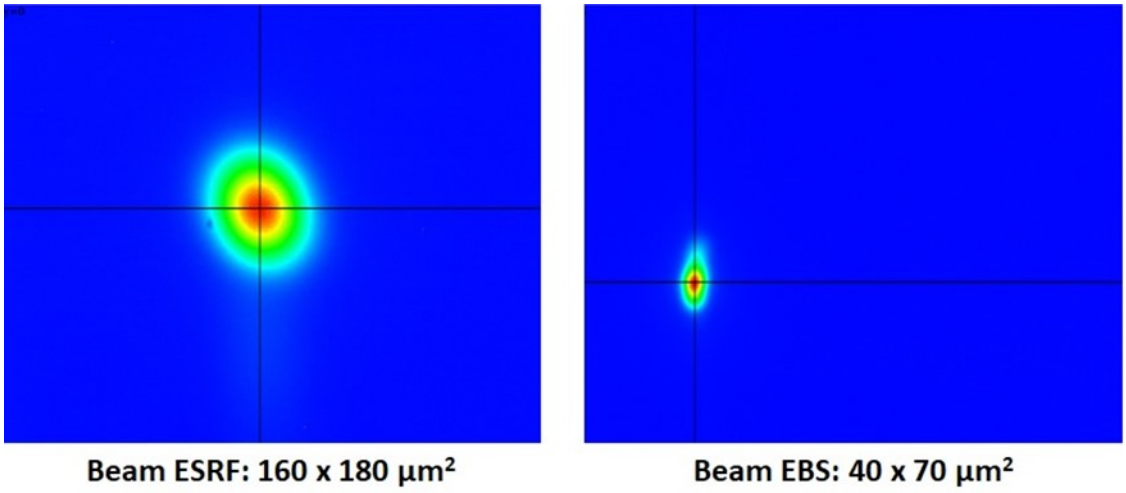

Figure 2: Beam size comparison between ESRF source (left) and EBS source (right). The measurements have been taken with a high-resolution camera.

Flux

The photon flux available on the sample from the new EBS ring has been measured for both Si (111) and Si(311) crystal pairs, with the mirrors on Si or Pt stripe. An ion chamber filled with N2 was used. The results are shown in Figure 3.

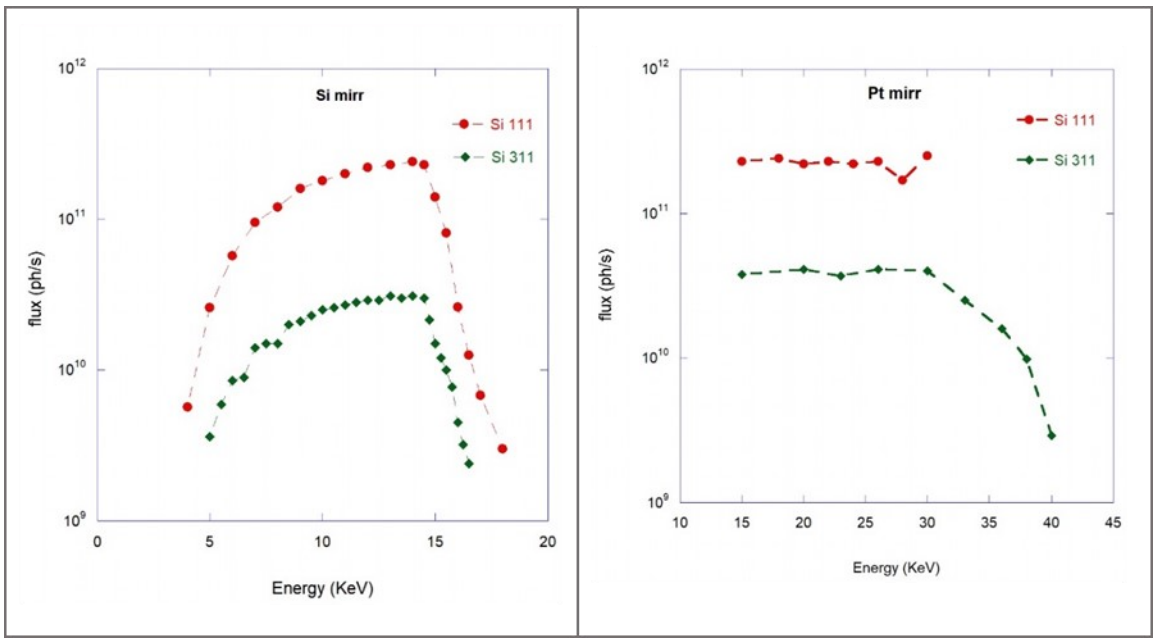

Figure 3: Flux available on the sample with Si(111) and Si(311) crystals, using a Si mirror (left) and a Pt mirror (right). Data have been measured with a storage ring current of 190 mA and principal slits open at 20 mm (H) and 1 mm (V).

Spectra acquisition in quick mode is now available at LISA, through a SPEC routine where the monochromator Bragg angle is moved continuously, while fast counting the ion chambers. A dedicated user GUI (Graphical User Interface) is also available (see Figure 4), which allows to choose the energy scan interval and the duration of scan. A complete EXAFS spectrum can be acquired in typically 1-2 minutes, the main limitation coming from the voltage-to-frequency converters.

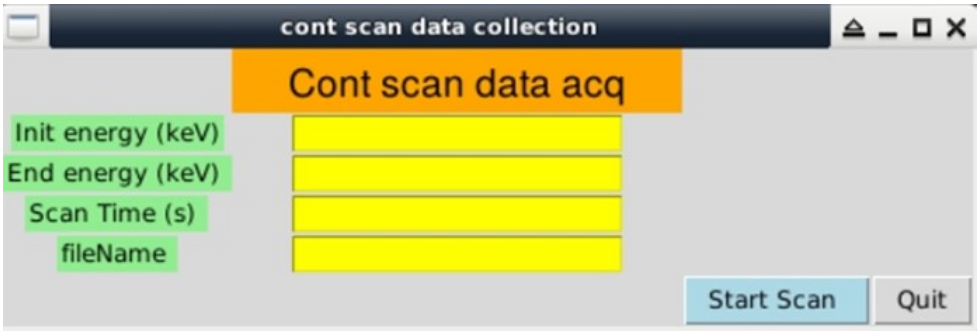

Figure 4: GUI for Quick XAS data collection.

Figure 5 shows three consecutive scans on a pellet of CuS, at Cu K-edge, the spectra reproducibility is quite good.

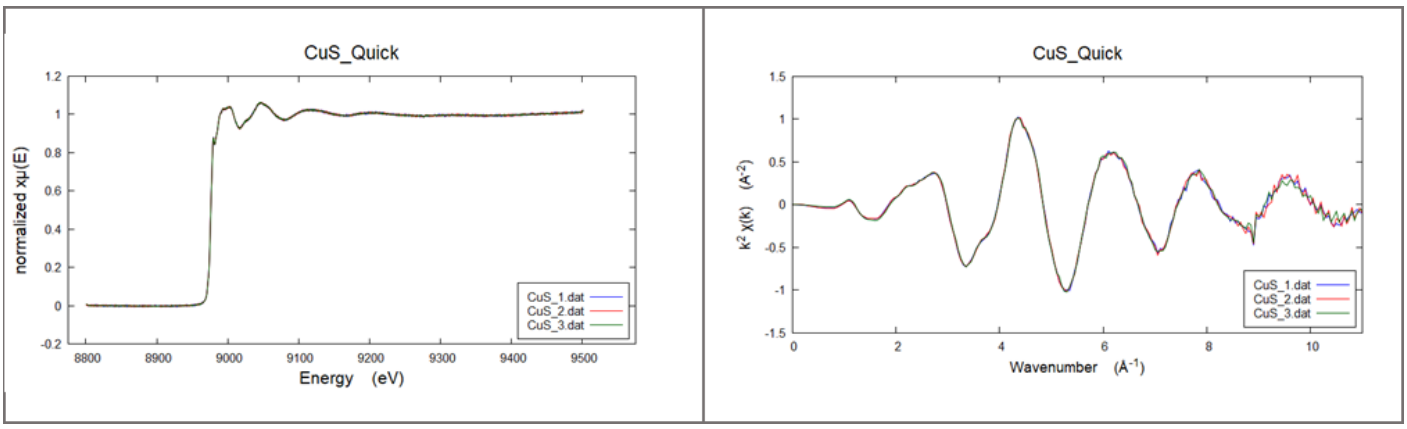

Figure 5: Three consecutive Cu K-edge Quick EXAFS scans of a CuS pellet. Left: raw spectra. Right: extracted EXFAS signal. Each spectrum was collected in 100 s.

2.3. Remote temperature control

Due to the considerable need of automatization of the data collection procedure consequent to the sanitary restrictions a remote Temperature control has been implemented. Now it is possible to collect spectra at different temperatures in automatic way, in the range 20 K to 400 K. A SPEC routine has been developed, which can change temperature, check temperature stability and perform the scans. A user GUI, shown in Figure 6, is available, which can collect spectra at up to six different temperatures automatically.

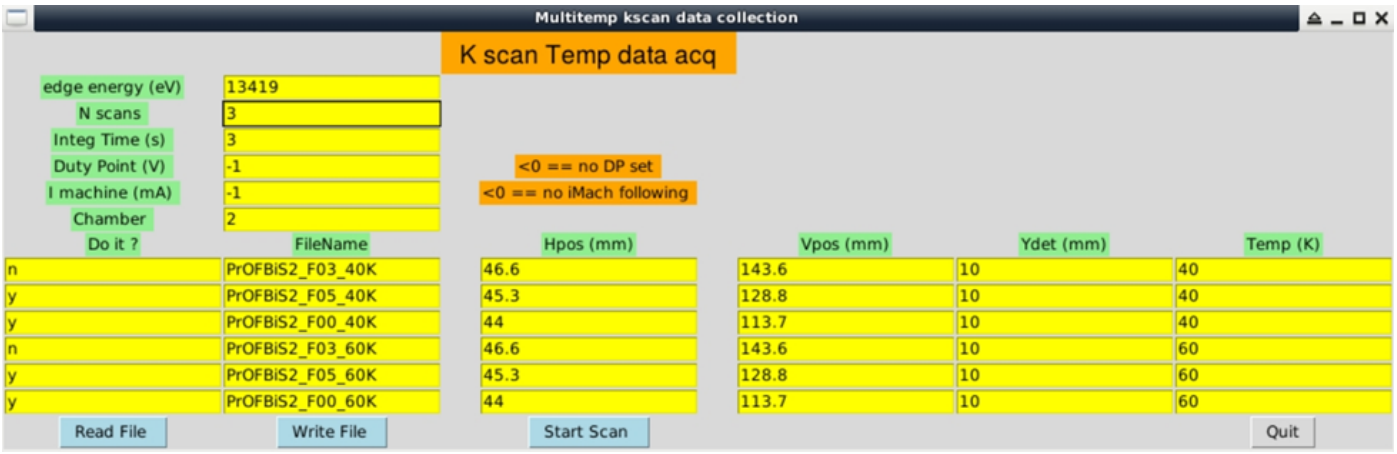

Figure 6: GUI for automatic temperature scans. The macro can acquire spectra for up to six temperatures in automatic way. The macro also checks temperature stability before starting the scans.

A. Puri

3.1.

Introducing Highly Redox-Active Atomic Centers into Insertion-Type Electrodes for Lithium-Ion Batteries

Y. Ma, [1,2] G. Giuli,[3] H. Euchner,[4] A. Groß,[4] G.O.Lepore,[5] F. d'Acapito,[5] D. Geiger,[6] J. Biskupek,[6] U. Kaiser,[6] H. M. Schütz,[1,2] A. Carlsson,[7] T. Diemant,[8] R. J. Behm,[1,8] M. Kuenzel,[1,2] S. Passerini,[1,2] D. Bresser[1,2]

[1]Helmholtz Institute Ulm, D., [2]Karlsruhe Institute of Technology (KIT), Karlsruhe, D., [3]School of Science and Technology, University of Camerino, I., [4]Institute of Theoretical Chemistry, Ulm University, D., [5]CNR-IOM-OGG, 38043 Grenoble, F., [6]Central Facility for Electron Microscopy, Ulm University, D., [7]Thermo Fisher Scientific, Eindhoven, NL., [8]Institute of Surface Chemistry and Catalysis, Ulm University, D.

In regard of the steadily increasing demand for enhanced energy and power densities for the next generation of rechargeable lithium-ion batteries, the development of new electrode materials, which are capable of hosting more lithium ions per unit weight and/or volume, is one of the main research directions in this field.

Ex situ X-ray absorption spectroscopy (XAS), in combination with a set of other complementary techniques, was used to investigate the reaction mechanism of a novel material: Fe-doped CeO_2 ($Ce_{0.9}Fe_{0.1}O_{2-\delta}$) as electrode for Li-ion batteries on LISA beamline. The results of the investigation indicate a new mechanism, which involves the reversible reduction of the Fe dopant at the atomic level.

The introduction of selected dopants such as Fe into the crystal structure of CeO_2 allows for an increase in capacity by up to 200%. While X-ray diffraction analysis for CeO_2 and $Ce_{0.9}Fe_{0.1}O_{2-\delta}$ indicate a classic solid-solution insertion-type de-/lithiation mechanism, it was not clear from these data what is the mechanism through which the introduction of Fe allows for much more Li^+ to be reversibly inserted.

To address this question, we performed an *ex situ* XAS investigation at the Ce L_{III}-edge and Fe K -edge of CeO_2 and $Ce_{0.9}Fe_{0.1}O_2$ before and after lithiation (Figure 2 a,b). For both materials, the data clearly reveal the reduction of Ce^{4+} to Ce^{3+}. In the case of Li-loaded $Ce_{0.9}Fe_{0.1}O_{2-\delta}$, the EXAFS data show that the incorporated Fe occupies an off-centered position in the cubic structure compared to Ce (Figure 2 d), and it is completely reduced to the metallic state, as highlighted by the comparison of the XANES data at the Fe K-edge (Figure 2 c). Furthermore, the *ex situ* EXAFS data (Figure 2 d,e) revealed that the metallic Fe in the lithiated state forms oligomers of about 2-4 Fe in close vicinity.

Summarizing all these findings, we propose the following model: beside the very homogeneous iron distribution, there are presumably always two Fe^{3+} cations in direct vicinity (as also shown by EXAFS fits), which is, in fact, reasonable with regard to the need of balancing the aliovalent doping induced point defects. In the reduced state, these iron atoms experience an increased attractive interaction, thus getting closer, without, however, destroying the crystalline host structure. Simultaneously, there are at least three Li^+ needed close to the Fe dopant to reduce it from Fe^{3+} to Fe^0, while its off-centred position allows for the required space.

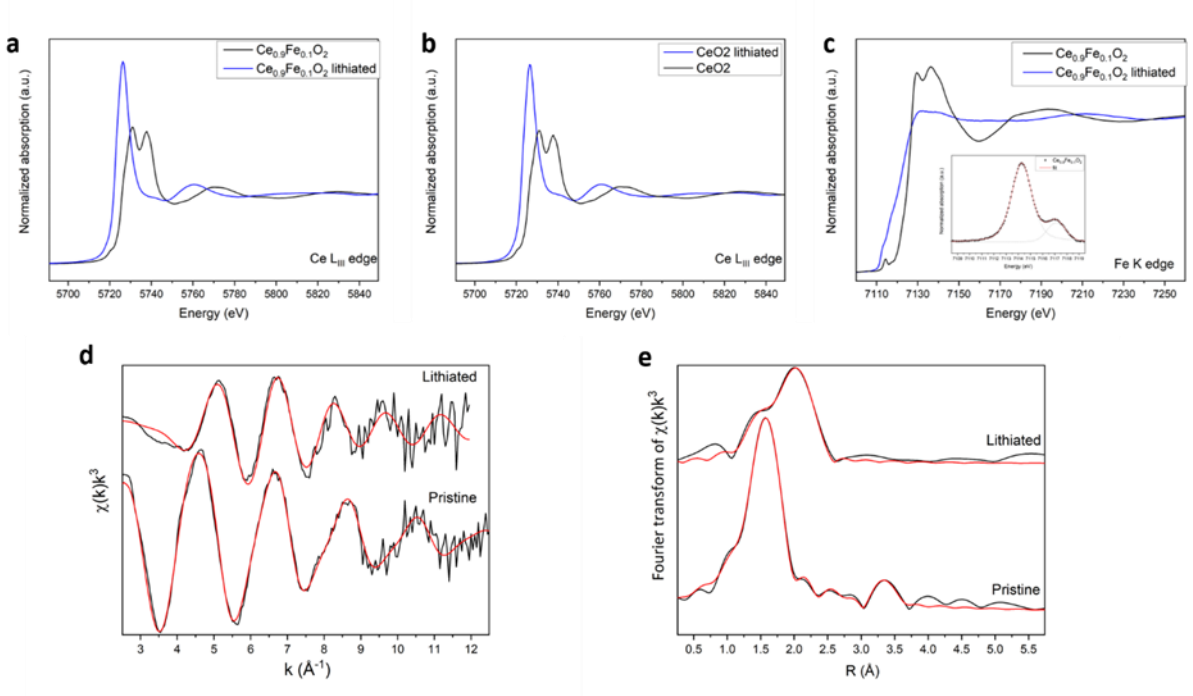

Figure 7: (a)-(c) Ex situ XANES data obtained for CeO2 and Ce0.9Fe0.1O2: The Ce LIII-edge for the pristine material and after lithiation for (a) CeO2 and (b) Ce0.9Fe0.1O2; (c) the Fe K edge for the pristine material and after lithiation. (d,e) Ex situ EXAFS spectra (black lines) and the corresponding multi-parameter fit (red lines) for pristine and lithiated Ce0.9Fe0.1O2.

In such a way, the available sites for lithium cations are substantially increased, which is eventually observed as the greatly enhanced Li^+ storage capability by about 200% compared to pure CeO_2.

Publication: [Adv. Energy Mater. **10** (2020), 2000783.]

Operando/In-situ X-ray absorption spectroscopy sheds light on composite phoelectrodes for photoelectrochemical water splitting.

M. Fracchia,[1] F. Malara,[2] A. Visibile,[3] T. Baran,[4] H. Kmentová,[5] D.Oliveira de Souza,[6] G. Aquilanti,[6] L.Olivi,[6] E. Ahlberg,[7] R. Psaro,[2] S. Rondinini,[3] A. Naldoni,[5] A. Vertova,[3] P. Ghigna,[1] A. Minguzzi[3]

[1]Dip. Chimica, Univ. Pavia, I-27100 Pavia, Italy, [2]CNR-ISTM, 20133 Milan, Italy, [3]Dip. Chimica, Univ. Milano, I-20133 Milano, Italy, [4] SajTom Ligh Future LTD,Wezerow 37/1, 32-090, Slomniki, Poland [5]Regional Centre of Advanced Technologies and Materials, Faculty of Science, Palacký University Olomouc, 78371 Olomouc, Czech Republic, [6] Elettra-Sincrotrone Trieste, 34149 Basovizza, Trieste, Italy, [7]Department of Chemistry and Molecular Biology, Gothenburg University, Kemivägen 4, 412 96 Göteborg, Sweden

Hydrogen is the most promising energy vector for the storage of energy from renewable sources, as demonstrated by its relevance in the recent European Union Green Deal. Among all proposed methods for clean hydrogen production, photoelectrochemical water splitting stands out for allowing the direct conversion of sunlight to high-purity H_2. Unfortunately, the technologic readiness level of this process is far for its commercialization and further research is needed to find the most suitable photoelectrode materials. The “core” of any photoelectrode is a visible-light absorbing semiconductor, either n- or p-doped, to serve as a photo-anode or -cathode, respectively. However, a semiconductor is not sufficient for guaranteeing an efficient light absorption, sufficient charge transfer and transport kinetics and high stability. Therefore, the coupling with under- or over-layers is needed towards an optimal composite photoelectrode. The design of such a complex system requires the detection and analysis of charge-transfer and transport dynamics between and within all different components. X-ray absorption spectroscopy is the method-of-choice to reach this goal, thanks to its ability in monitoring the average charge state and local structure of a given element, even in complex systems and under operative conditions. [1,2,3]

In recent works, we investigated two different systems, namely a photocathode based on Cu_2O (cuprous oxide) and a α-Fe_2O_3 (hematite)-based photoanode. In the first case, the semiconductor was deposited onto fluorine-doped tin oxide without and with a Cu or Au underlayer, the latter leading to a great increase in the photocurrent, due to an improved charge transport. As shown in Figure 2 (panels a,b), both XANES and EXAFS demonstrate that there are no significant differences in the structural parameters of the different samples, demonstrating that the presence/absence of the underlayer does not change the local chemical surrounding of Cu_2O. This important finding leads to the conclusion that the underlayer improves the activity without influencing the structure of the semiconductor, thus making the design of composite systems more predictable. In addition, a Cu/Cu_2O photoelectrode can be electrodeposited from a single bath in two steps by simply shifting the deposition potential. In the second case, hematite photoanodes were modified by depositing NiOOH overlayers with the aim of improving charge transfer kinetics at the solid/electrolyte interface. However, striking differences in the photocurrent intensities were observed as a function of the overlayer thickness. A combined use of electrochemical impedance spectroscopy and operando/in-situ XANES and fixed energy X-ray absorption voltammetry (FEXRAV[4]) revealed that the activity of the photoelectrode can be limited by the diffusion of holes using an 80 nm thick NiOOH layer, where the oxidation state of Ni increased up to +4 under illumination and a sufficiently positive applied bias. This is shown in Figure 2 (panel c), where the spectrum at the Ni K-edge of the electrode at 1.3 V vs RHE under illumination shows a notable shift towards higher energies with respect to dark condition.

Moreover, the absorption coefficient was recorded at a fixed energy of 8350 eV and at 1.3 V while switching alternatively on and off the light (Figure 8 panel d, black line); μ shows a net decrease upon illumination, indicating the partial oxidation of the thick NiOx layer. Oppositely, adopting a thin NiOOH layer (a few nm), the oxidation state of Ni undergoes negligible changes, since holes are easily transferred through the overlayer (where they do not accumulate) and across the interface. This finding is the key for the understanding of the electronic relations between the semiconductor and the overlayer and will serve as the basis for the design of new materials, towards a highly efficient solar-to-hydrogen conversion.

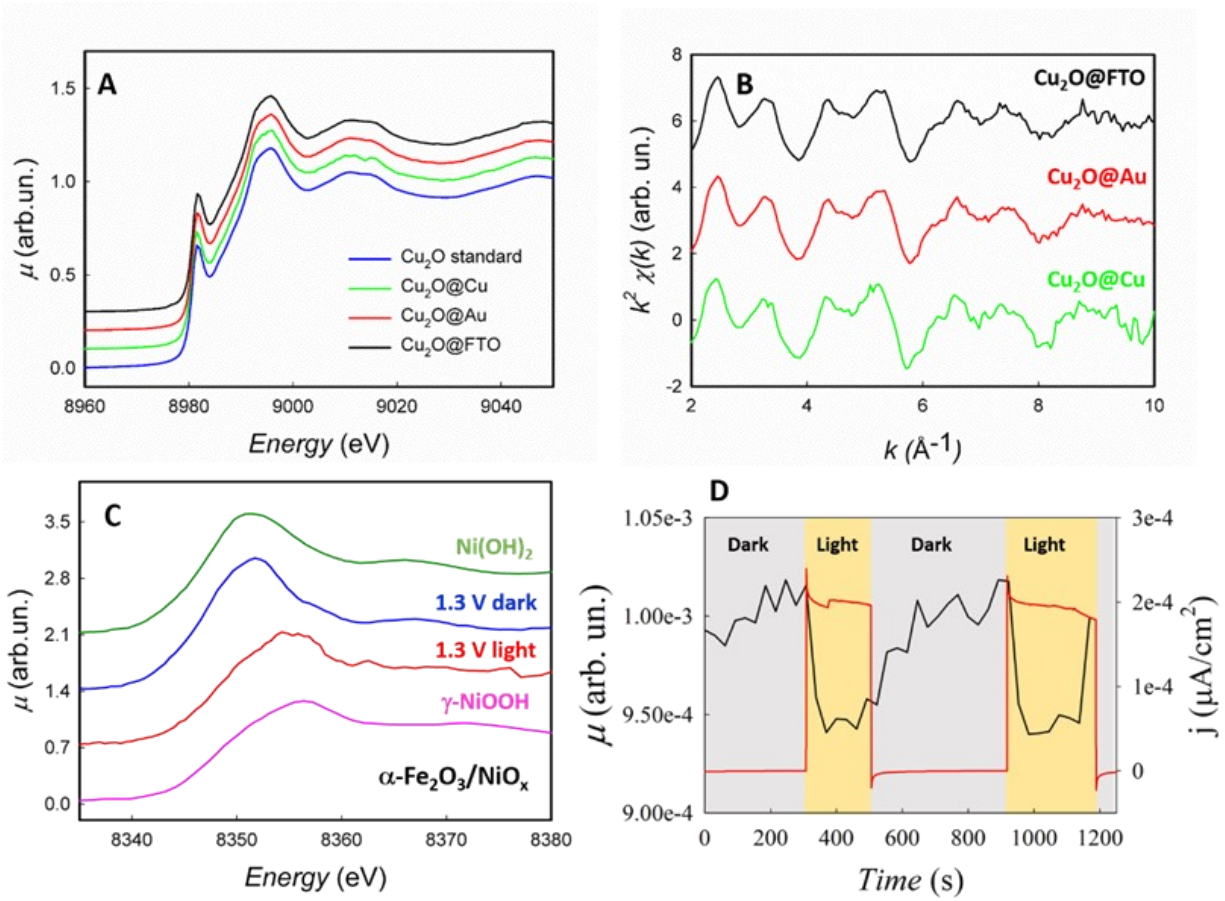

Figure 8: a) XANES spectra at the Cu K-edge for Cu2O photocathodes without underlayer (black line) and with Au (red line) and Cu (green line) underlayer, respectively b) Comparison of the EXAFS signals for the three Cu2O photocathodes. As evident by this figure, no significant differences are detected in the three cases. c) XANES spectra at the Ni K-edge for a-Fe2O3/NiOx electrode with high NiOx thickness (80 nm) at 1.3 V vs RHE with (red line) and without (blue line) illumination. The XANES spectra of Ni(OH)2 and γ-NiOOH are also shown for comparison. d) X-ray absorption coefficient (μ) at a fixed energy of 8350 eV and photocurrent density at a fixed potential (1.3 V) acquired simultaneously, switching the light on and off.

Publication: [J. Solid State Electrochem. **24** (2020), 339-355, ACS Catal. **10** (2020), 10476-10487.]

References:

(1) T. Baran et al., Electrochim. Acta **207** (2016), 16-21
(2) M. Fracchia et al., Surfaces **1** (2018), 138-150
(3) E. Achilli et al. J. Synchrotron Radiat. **23** (2016), 622-628
(4) A. Minguzzi et al., Anal. Chem. **85** (2013), 7009-7013.

Short-range chemical order and local lattice distortion in a compositionally complex alloy

A. Fantin[1,2], G. O. Lepore[3], A. M. Manzoni[2,4], S. Kasatikov[2,5], T. Scherb[2], T. Huthwelker[6], F. d'Acapito[3], G. Schumacher[1,2].

[1]Technische Universität Berlin, [2]Helmholtz-Zentrum Berlin, [3]CRG-IOM-OGG c/o ESRF, [4]Bundesanstalt für Materialforschung und - prüfung, [5]Saint-Petersburg State University, [6]Paul-Scherrer-Institute

High entropy alloys (HEA), medium entropy alloys and multi-phase compositionally complex alloys (CCA) have gained much attention in the last 20 years because of their outstanding mechanical properties. Such baseless alloys provide different open questions on local chemical ordering, lattice distortions, orbital hybridization and/or charge transfer which define the very nature of alloys' mechanical properties. By combining EXAFS measurements in the tender X-ray range (PHOENIX-SLS, Al K-edge) and at higher X-ray energies (BM08-ESRF, transition metal K -edges), local chemical ordering in a CCA, $Al_8Cr_{17}Co_{17}Cu_8Fe_{17}Ni_{33}$ was quantified showing preferred Al-Ni and Al-Cu pairs (see Figure 9). In addition, slight structural distortions, much lower than the predicted ones of metallic radii, were found.

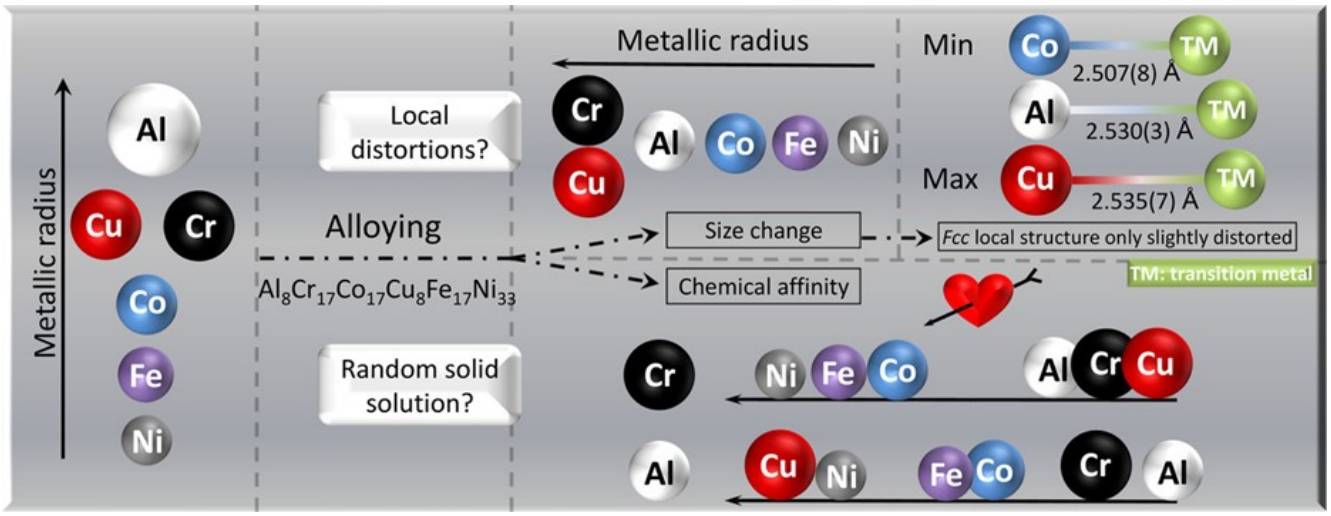

Figure 9: Graphical abstract resuming the main findings: Al shrinks its metallic radius upon alloying and subsequently reducing the high entropy alloy unit cell distortions. Clear chemical affinities in the alloy with Al-Cu and Al-Ni the preferred pairs. Reprinted from Fantin et al.: short-range chemical order and local lattice distortion in a compositionally complex alloy, Vol. 193, Pages 329-337, with permission of Elsevier.

Local distortions and short-range order are the keys to understand the solid solution mechanical behavior of the novel material class of HEA, more than the individual properties of alloying elements, such as atomic radius or shear modulus. Low energy X-ray absorption spectroscopy performed at PHOENIX beamline, together with BM08 (ESRF) data allowed obtaining local structure information on a chosen compositionally complex alloy, $Al_8Cr_{17}Co_{17}Cu_8Fe_{17}Ni_{33}$, especially highlighting the role of Al. XAS provided qualitative information about the electronic structure and quantitative information on local structure and partial chemical ordering: Al short-range chemical ordering and local lattice distortions in $Al_8Cr_{17}Co_{17}Cu_8Fe_{17}Ni_{33}$ were identified and quantified experimentally for the first time in a compositionally complex alloy. EXAFS analysis identified local distortions and a higher affinity of Al for heavier 3d metals, with Cu-Al being the preferred pair.

The amount of local distortions in $Al_8Cr_{17}Co_{17}Cu_8Fe_{17}Ni_{33}$ cannot result in lattice distortions in the *fcc* unit cell larger than ~0.04 Å. These values are much smaller than those predicted solely by atomic radii considerations. The Al metallic radius in the $Al_8Cr_{17}Co_{17}Cu_8Fe_{17}Ni_{33}$ is estimated to be of the same order than the average transition metal one, i.e. 1.26 Å, much lower than the tabulated value of 1.43 Å of pure Al. Al reduces its metallic radius in order to accommodate into the lattice, lessening its distortion. Two important points in the characterization of HEA, namely local chemical ordering and local lattice distortions, were clarified providing a tool to answer the open questions reported in recent reviews.

Publication: [Acta Materialia **193** (2020), 329-337]

Amorphous intermixing of noble and magnetic metals in thin film-based nanostructures

C. Maurizio [1], N. Michieli[1], B. Kalinic[1], C. Scian[1], V. Mattarello[1], G. Ciatto[2], G. Mattei[1]

[1]Physics and Astronomy Department, University of Padova, Italy [2]SOLEIL Synchrotron- France

In nanostructures made of a mixture of bulk-immiscible metallic species, the alloy formation down to the atomic scale is a crucial and debated point.

In this work we have reported on the first experimental evidence of an amorphous metallic phase in Au-Co that is formed on a Au+Co cosputtering deposition performed at room temperature. Flat thin films have been investigated, together by 2D ordered arrays of nanostructures obtained by coupling physical vapour deposition with annosphere lithography. In particular, two SEM images of a 2D hexagonal array of Au-Co seminanoshells (SNS) covering polystyrene nanospheres are reported in Figure 10.

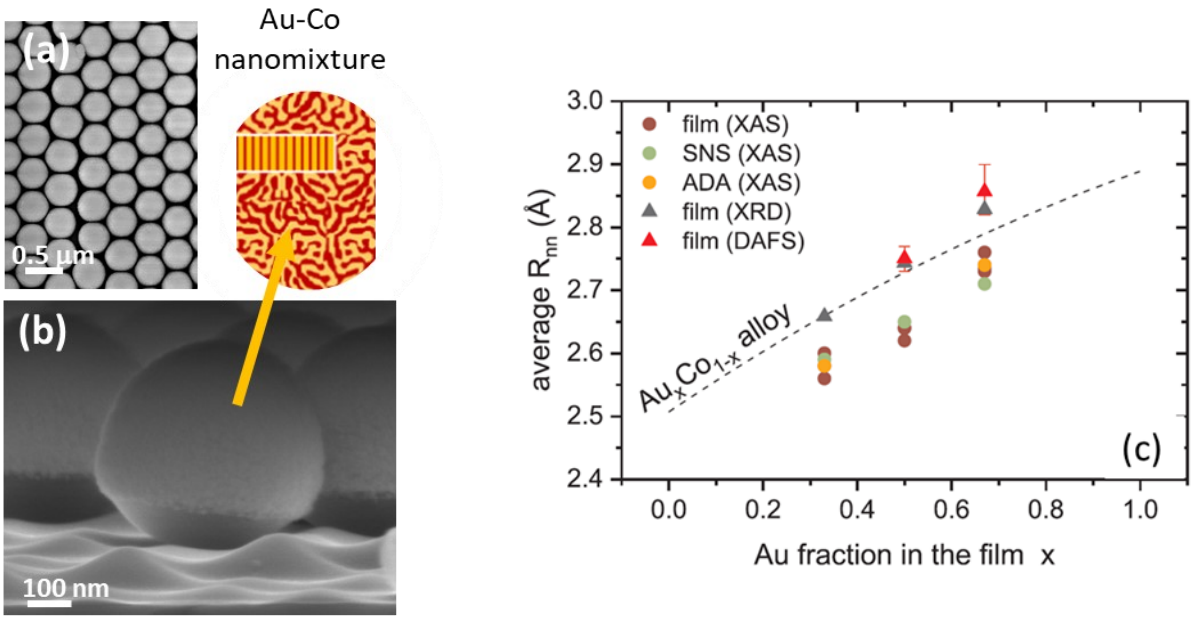

2.3.1.2

Figure 10: (a,b) FE-SEM images of the (seminanoshells (SNS) + antidot arrays (ADA)) layer obtained by Au-Co deposition (Au/Co = 1) on a 2D array of etched polystyrene nanospheres: (a) top view and (b) cross view. In (b) the Au-Co seminanoshell covering one polystyrene nanosphere is visible, as well as the underneath anti-dot array on the substrate. (c) Nearest neighbor interatomic distances versus the fraction of Au atoms in the deposited (nanostructured) film. Black dashed line shows the values for the crystalline − AuxCo1-x alloy (Vegard's law). The results from XRD and DAFS (30 nm thick films) are also reported (black and red triangles, respectively).

To investigate the local structure of the produced film-based nanostructures, a X-ray Absorption Spectroscopy (XAS) experiment was performed in fluorescence mode at 80 K at Au L3 and Co K -edges, at the Italian beamline BM08 of the ESRF synchrotron. EXAFS data analysis focused on the first coordination shell, considering at Co-edge (Au-edge) both a Co-Co (Au-Au) coordination and a Co-Au one (whose distance and Debye Waller-DW factors where imposed to be the same when measured at Co- or Au- edge spectrum).

The main results of the EXAFS analysis are reported in Figure 2.3.1.2, where the first shell distance R, obtained as a weighted average over the different atomic contributions (Au-Co, Au-Au and Co-Co) is reported as a function of the average composition of the deposited layer. R mainly depends on the average composition and not on the kind of produced nanostructures (SNS, Antodot arrays-ADA or flat film). Moreover, R is significantly different from the value retrieved by XRD in grazing incidence mode. These data have been combined with a Diffraction Anomalous Fine Structure (DAFS) experiment (SOLEIL synchrotron), where results very similar to standard diffraction are obtained (red markers in 10). The analysis shows that in all the investigated nanostructures (thin films and 2D-ordered arrays) Au and Co are finely mixed, but at the sub-nanometer length scale separate Au and Co domain exists. Nevertheless, the fine mixing leads to an extended Au-Co interface that is responsible for the previously measured magnetic moment of Au atoms. The major amorphous part, characterized in detail here for the first time, very likely forms also when other preparation routes are considered, and is intimately related to the different atomic radii and to the immiscibility of the two metals. A minor fraction of fcc solid solution nanoalloy, coexisting with the amorphous part, has also been evidenced. The thermal stability of the alloy (amorphous and crystalline) is limited to about 250°C.

These results are expected to help to correlate the atomic structure of the Au- Co nanoalloys with their properties (in particular magnetic, but not exclusively), which are relevant for possible applications of these materials.

Publications: [Maurizio C., et al. Applied Surface Science **513** (2020), 145779-1-8, Maurizio C., et al. Surface & Coatings Technology **385**, (2020), 125309-1-5 (2020)]

The fate of CdS Quantum Dots in A. Thaliana as revealed by EXAFS

M. Marmiroli[1], G. O Lepore[2], L. Pagano[1], F. d'Acapito[2], A. Gianoncelli[3], M. Villani[4], L. Lazzarini[4], J. C. White[5], N. Marmiroli[1]

1 Dept. Chemistry, Life Science and Environmental sustainability, University of Parma, Italy. 2 CNR-IOM-OGG c/o ESRF, Grenoble, France. 3 Elettra - Sincrotrone Trieste, Italy. 4 IMEM-CNR, Parma, Italy. 5 The Connecticut Agricultural Experiment Station, New Haven, CT, USA.

CdS-based QDs are increasingly used nanomaterials as components for fluorescent imaging, biosensing, LED screens and solar power cells. Their release into the environment is consequently expected, leading to some concern about their interactions with biota.
Model plant *Arabidopsis thaliana* wild type (wt) and two mutant lines (*at*np01 and *at*np02) known to be tolerant to CdS QDs but not $CdSO_4$ were exposed to CdS QDs or $CdSO_4$ at sub-inhibitory concentrations. Plants treated with CdS QDs accumulated significantly less Cd than those treated with $CdSO_4$, even though the effective amount of Cd administered as QDs was higher than that administered as salt.
EXAFS analysis (Figure 11, left) were performed on LISA beamline and revealed a complex environment for Cd in the samples, with Cd bonded to both S and O atoms in plants grown on CdS QDs and $CdSO_4$. No differences are found between the wild type and the mutant lines. On the other hand, Cd coordination differs depending on the type of Cd exposure. Cd-O distances vary from ≅2.16 Å (CdS QDs) to ≅2.22 Å ($CdSO_4$). Cd-S bonds are strongly favoured in plants grown on CdS QDs, while, in plants grown on $CdSO_4$, CdO and CdS bonds are equally distributed.
On this basis the following scheme for the interaction between CdS QDs and *Arabidopsis thaliana* can be inferred (Figure 11, right)

I. CdS QDs are partially biotransformed after their uptake and Cd atoms are not released as Cd^{2+} ions. The cellular response generates reactive oxygen species (ROS).
II. ROS may impact other organs if an anti-oxidative stress tolerance response is not triggered.
III. The bio-modified nanostructures form stabilizing bonds with S and O atoms present within defense molecules produced as a consequence of the increased ROS production.

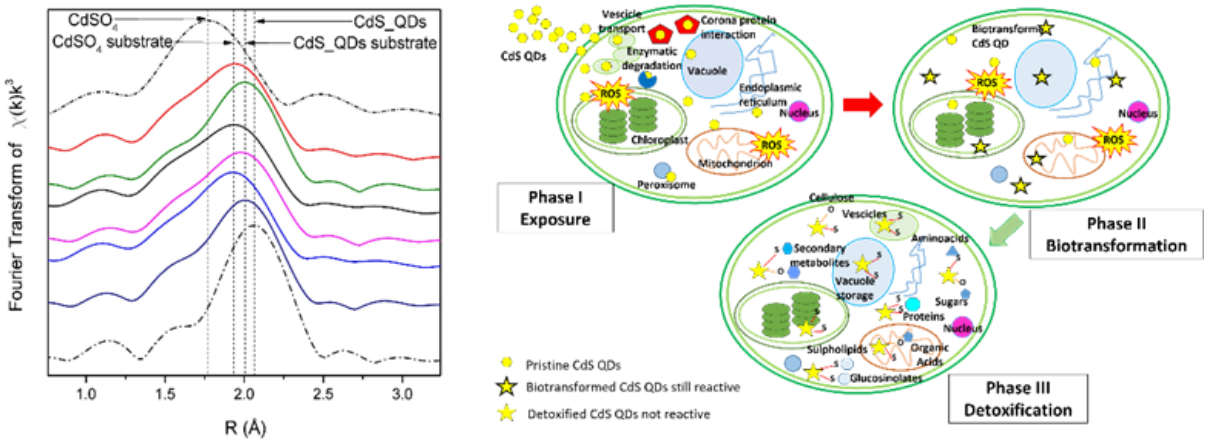

Figure 11: left) EXAFS Fourier transform spectra of studied samples and reference compounds; right) Schematic of the CdS QDs from uptake to detoxification within the plant cell. O, S and Cd are oxygen, sulphur and Cd2+ atoms, respectively, yellow circles = CdS QDs, yellow stars with thick border line = biotransformed CdS QDs, yellow stars with thin border line = bound particles left from the biotransformation.

Publication: [Environ. Sci. Nano **7.4** (2020), 1150-1162.]

1 d'Acapito F., Kowalczyk P., Raty J.Y., Sabbione C., Hippert F., Noé P. - Local structure of [(GeTe)2/(Sb2Te3)m]n super-lattices by X-ray absorption spectroscopy Journal of Physics D 53, 404002-1-404002-8(2020)

2 D'Orazio M., Campanella B., Bramanti E., Ghezzi L., Onor M., Vianello G., Vittori-Antisari L., Petrini R. - Thallium pollution in water, soils and plants from a past-mining site of Tuscany: Sources, transfer processes and toxicity Journal of Geochemical Exploration 209, 106434-1-106434-14(2020)

3* Fantin A., Lepore G.O., Manzoni A.M., Kasatikov S., Scherb T., Huthwelker T., d'Acapito F., Schumacher G. - Short-range chemical order and local lattice distortion in a compositionally complex alloy Acta Materialia 193, 329-337(2020)

4 Kesavan J.K., Scardi P., Stavrinadis A., Agkul M.Z., Burgues-Ceballos I., Konstantatos G., Boscherini F. - Cation disorder and local structural distortions in AgxBi1–xS2 nanoparticles Nanomaterials 10, 316-1-316-13(2020)

5 Kuznetsov A.V., Churkin O.A., Popov V.V., Shchetinin I.V., Ivanov A.A., Yastrebtsev A.A., Gaynanov B.R., Chernysheva O.V., Puri A., Alekseev P.A., Menushenkov A.P. - Magnetization of crystalline and amorphous phases of R2Ti2O7 and R2Zr2O7 (R = Gd, Dy, Tb) Journal of Superconductivity and Novel Magnetism 33, 2395–2404(2020)

6* Ma Y., Ma Yu., Giuli G., Euchner H., Gross A., Lepore G.O., d'Acapito F., Geiger D., Biskupek J., Kaiser U., Schütz H.M., Carlsson A., Diemant T., Behm R.J., Kuenzel M., Passerini S., Bresser D. - Introducing highly redox-active atomic centers into insertion-type electrodes for lithium-ion batteries Advanced Energy Materials 10, 2000783-1-2000783-13(2020)

7* Malara F., Fracchia M., Kmentová H., Psaro R., Vertova A., Oliveira de Souza D., Aquilanti G., Olivi L., Ghigna P., Minguzzi A., Naldoni A. - Direct observation of photoinduced higher oxidation states at a semiconductor/electrocatalyst junction ACS Catalysis 10, 10476-10487(2020)

8* Marmiroli M., Lepore G.O., Pagano L., dacapito f., Gianoncelli A., Villani M., Lazzarini L., White J.C., Marmiroli N. - The fate of CdS quantum dots in plants as revealed by eExtended X-ray Absorption Fine Structure (EXAFS) analysis Environmental Science: Nano 7, 1150-1162 (2020)

9 Maurizio C., Mattarello V., Kalinic B., Michieli N., Balasa I.G., Scian C., Mattei G. - Structural modification of Au-Co thin films induced by annealing in oxidizing atmosphere Surface & Coatings Technology 385, 125309-1-125309-5(2020)

10 Maurizio C., Michieli N., Kalinic B., Mattarello V., Scian C., Ciatto G., Mattei G. - Amorphous intermixing of noble and magnetic metals in thin film-based nanostructures Applied Surface Science 513, 145779-1-145779-8(2020)

11* Noé P., Verdy A., Dory J.B., Bernard M., Navarro G., Jager J.B., Gaudin J., Raty J.Y. - Toward ultimate nonvolatile resistive memories: The mechanism behind ovonic threshold switching revealed Science Advances 6, eaay2830-1- eaay2830-11(2020)

12 Palumbo O., Manzi J., Meggiolaro D., Vitucci F.M., Trequattrini F., Curcio M., Paolone A., Brutti S. - Effect of transitional metals (Mn and Ni) substitution in LiCoPO4 olivines Molecules 25, 601-1-601-15(2020)

13 Petroselli C., Moroni B., Crocchianti S., Selvaggi R., Soggia F., Grotti M., d'Acapito F., Cappelletti D. - Iron speciation in different saharan dust advections and effect of the procedural blank on the results from X-ray absorption spectroscopy and selective leaching experiments Atmosphere 11, 735-1-735-14(2020)

14 Rezvani S.J., Mijiti Y., Gunnella R., Nobili F., Trapananti A., Minicucci M., Ciambezi M., Bresser D., Nannarone S., Passerini S., Di Cicco A. - Structure rearrangements induced by lithium insertion in metal alloying oxide mixed spinel structure studied by x-ray absorption near-edge spectroscopy Journal of Physics and Chemistry of Solids 136, 109172-1-109172-8(2020)

15 Righi L., Merlini M., Gemmi M. - High-temperature evolution of the incommensurate composite crystal Ca0.83CuO2 Crystals 10, 630-1-630-11(2020)

16 Soffientini A., Ghigna P., Spinolo G., Boldrini S., Famengo A., Tamburini U.A. - Nanostructured calcium cobalt oxide Ca3Co4O9 as thermoelectric material. Effect of nanostructure on local coordination, Co charge state and thermoelectric properties Journal of Physics and Chemistry of Solids 143, 109474-1-109474-10(2020)

17* Tadayon M., Younes-Metzler O., Shelef Y., Zaslansky P., Rechels A., Berner A., Zolotoyabko E., Barth F.G., Fratzl P., Bar-On B., Politi Y. - Adaptations for wear resistance and damage resilience: Micromechanics of spider cuticular "tools" Advanced Functional Materials 30, 2000400-1-2000400-13(2020)

18 Verdy A., d'Acapito F., Dory J.B., Navarro G., Bernard M., Noé P. - Effect of nitrogen on the amorphous structure and subthreshold electrical conduction of GeSeSb-based ovonic threshold switching thin films Physica Status Solidi-Rapid Research Letters 14, 1900548-1-1900548-7(2020)

19 Visibile A., Fracchia M., Baran T., Vertova A., Ghigna P., Ahlberg E., Rondinini S., Minguzzi A. - Electrodeposited Cu thin layers as low cost and effective underlayers for Cu2O photocathodes in photoelectrochemical water electrolysis Journal of Solid State Electrochemistry 24, 339-355(2020)

5. Contacts

Beamline responsible:	Francesco d'Acapito dacapito@esrf.fr +33 4 7688 2426 , +33 6 8936 4302
Beamline scientist:	Alessandro Puri puri@esrf.fr +33 4 7688 2859
Local Contact:	+33 6 8838 6994
Beamline:	+33 4 7688 2085
Laboratory:	+33 4 7688 2743
Skype:	gilda_beamline
Administration:	Fabrizio La Manna lamanna@esrf.fr +33 4 7688 2962
Web page:	http://www.esrf.eu/UsersAndScience/Experiments/CRG/BM08/

Forthcoming proposals submission deadlines

ESRF quota: March 1st 2021, beginning September 2021
CERIC quota: March / October 2021 (exact date to be defined)

6. Contributors to this issue

F. d'Acapito, A. Puri, (CNR-IOM, Grenoble), R. De Donatis (CNR, Genova), A. Fantin (TU Berlin), G. O. Lepore (Univ. Firenze), C. Maurizio (Univ. Padova), A. Minguzzi (Univ. Milano).